
Effective Interplay between Sparsity and Quantization: From Theory to Practice

Simla Burcu Harma
EcoCloud, EPFL
simla.harma@epfl.ch

Ayan Chakraborty
EcoCloud, EPFL
ayan.chakraborty@epfl.ch

Elizaveta Kostenok
EcoCloud, EPFL
elizaveta.kostenok@epfl.ch

Danila Mishin
EcoCloud, EPFL
danila.mishin@epfl.ch

Dongho Ha
Yonsei University
dongho.ha@yonsei.ac.kr

Babak Falsafi
EcoCloud, EPFL
babak.falsafi@epfl.ch

Martin Jaggi
EcoCloud, EPFL
martin.jaggi@epfl.ch

Ming Liu
Google
miliu@google.com

Yunho Oh
Korea University
yunho_oh@korea.ac.kr

Suvinay Subramanian
Google
suvinay@google.com

Amir Yazdanbakhsh
Google DeepMind
ayazdan@google.com

Abstract

The increasing size of deep neural networks necessitates effective model compression to improve computational efficiency and reduce their memory footprint. Sparsity and quantization are two prominent compression methods that have individually demonstrated significant reduction in computational and memory footprints while preserving model accuracy. While effective, the interplay between these two methods remains an open question. In this paper, we investigate the interaction between these two methods and assess whether their combination impacts final model accuracy. We mathematically prove that applying sparsity before quantization is the optimal sequence for these operations, minimizing error in computation. Our empirical studies across a wide range of models, including OPT and Llama model families (125M-8B) and ViT corroborate these theoretical findings. In addition, through rigorous analysis, we demonstrate that sparsity and quantization are *not* orthogonal; their interaction can significantly harm model accuracy, with quantization error playing a dominant role in this degradation. Our findings extend to the efficient deployment of large models in resource-limited compute platforms and reduce serving cost, offering insights into best practices for applying these compression methods to maximize efficacy without compromising accuracy.¹

1 Introduction

Recent breakthroughs in deep neural networks (DNNs) have surpassed human-level capabilities across various tasks such as text generation, machine translation, and computer vision. However, this success comes with significant challenges due to the exponential growth in the size and complexity of DNN models and datasets [3, 69, 52, 58, 1, 57, 25, 46, 37], which complicates their practical deployment and efficient serving. Delivering efficient and real-time inference for these large models is constrained by arithmetic density (throughput/silicon area [11, 6, 20]), memory footprint, and the pressure on memory bandwidth across various hardware platforms (e.g. GPU [45], TPU [43]).

¹Code and data are available at: <https://bit.ly/quantization-sparsity-interplay>

Among various efficiency efforts, model compression has emerged as a crucial solution to effectively address the challenges associated with large models [38, 11, 60, 6, 4, 70, 66, 20, 49, 50, 21, 31, 16, 27, 30, 29] with quantization standing out as a prominent method in terms of overall compression ratio. Quantization effectively reduces the precision of model tensors from native floating-point representation to formats such as FP16 [38], BFloat16 [60], INT8 [59, 68], and others [11, 6, 4, 70, 66, 20, 49, 50].

To further enhance compression, researchers often use sparsity, pruning elements of tensors that are least significant to model accuracy. This reduction in parameters decreases the memory footprint of models and potentially improves computational efficiency by eliminating unnecessary computations [56]. Sparsity methods typically prune elements of a tensor based on their magnitudes (a proxy for the importance of an element to model accuracy) [19, 42, 34, 9, 2]. Magnitude-based sparsity, especially when combined with fine-tuning, offers straightforward implementation and the potential to achieve noticeable compression rates with negligible impact on accuracy [28, 51].

While prior work has extensively studied the impact of sparsity and quantization in isolation, their combined impact is less explored. A few studies [18, 61, 33] suggest that the combination of these two methods does *not* significantly hurt accuracy. Unfortunately, these studies either primarily focus on CNNs [18] or do not fully investigate the potential combined impact because they exclusively quantize weight tensors while keeping activations in high precision [61, 33].

In this paper, we aim to systematically study the interplay between quantization and sparsity. Quantization and sparsity leverage two fundamentally separate computational properties of DNNs, presenting an opportunity for their combined use. However, their combined impact on model accuracy involves complex dynamics due to the introduction of errors in tensors. We hypothesize that the interplay between quantization and sparsity can result in additional errors, based on the following insights. **First**, applying quantization before sparsity (Q→S) may adversely disrupt the relative importance of tensor elements, potentially leading to the removal of significant elements of a tensor. **Second**, applying sparsity before quantization (S→Q) can introduce additional errors in dot product calculations, as these are influenced by the magnitudes and precision of the involved elements. To the best of our knowledge, we are the first to study the interplay between quantization and sparsity in depth, to identify the conditions under which accuracy can be preserved or compromised. Our contributions are summarized below:

- **Theoretical Analysis of Sparsity-Quantization Interplay:** We provide the first in-depth theoretical analysis of how sparsity and quantization interact. Our mathematical proofs establish that applying sparsity *before* quantization (S → Q) is the optimal sequence for compression.
- **Non-orthogonality and Error Dynamics of Compression Methods:** We mathematically demonstrate that sparsity and quantization are *not* orthogonal operations. Combining them introduces additional errors beyond the sum of their individual errors. We analyze the specific error dynamics arising from this interaction, highlighting the dominant role of quantization error in the overall degradation of model accuracy.
- **Extensive Empirical Study:** We validate our theoretical findings through extensive experiments covering a diverse range of models, including prominent LLMs (OPT, LLaMA) and ViTs. These experiments support our hypotheses about the optimal order of compression operations and underscore the non-orthogonality of sparsity and quantization, affirming the practical relevance of our theoretical analysis. Our experiments demonstrate that applying quantization and sparsity in a sub-optimal order can cause up to 7.96 point increase in perplexity.

2 Related work

Quantization. The ever-growing size of DNN models has spurred extensive research into using narrow numerical formats for inference to reduce memory footprint and improve computational efficiency [38, 11, 60, 6, 4, 70, 66, 20, 49, 50]. Numerical formats employ scaling factors to adjust their dynamic range and can be categorized based on the granularity and their levels. Table 3 in AppendixA summarizes the most common numerical formats.

Sparsity. Sparsity methods [21, 31, 16, 27, 30] aim to reduce computational and storage overhead in DNNs by selectively eliminating tensor elements according to various sparsity mask selection criteria.

Broadly, these methods fall into two main categories based on sparsity patterns: unstructured [18, 17, 13, 12] and structured [62, 65, 26, 42, 48, 71, 54, 24, 34].

Combining quantization and sparsity. Prior work has studied the combination of quantization and sparsity and its impact on model performance: sparsity followed by quantization [67, 15, 14, 47, 42, 32, 18] and quantization followed by sparsity [23, 22, 63, 42]. There are two missing pieces of information from these pieces of prior work. First, consensus on the optimal order of compression operations is not clear. Some favor one order without clear justification, while others treat the methods as independent compression schemes. Second, there is lack of theoretical grasp on how sparsity and quantization errors interact and influence final model performance. Appendix A covers additional related work.

3 Mathematical analysis of orthogonality of quantization and sparsity

This section provides a mathematical analysis of the interplay between quantization and sparsity, formalizing these compression methods and examining their composition at both the tensor and dot product levels. Our analysis centers on quantization methods that reduce the bit-width of model weights and activations using block-wise numerical formats, which are prevalent in practical implementations [6, 11, 70, 49, 50, 40]. These formats determine the scaling factor based on the maximum element within a block of elements. We denote a quantization method employing these numerical formats as *max-scaled block-wise quantization*. We use magnitude-based sparsity for both unstructured and N:M structured sparsity.

Definition 3.1 (Max-scaled block-wise quantization). Let $\mathbf{x} \in \mathbb{R}^n$ be a block of n numbers and $m \in \mathbb{N}$ denotes the quantization bit-width. Max-scaled block-wise quantization $q : \mathbb{R}^n \rightarrow \mathbb{R}^n$ is a transformation of the block \mathbf{x} such that

$$x_i \xrightarrow{q} Q_m(x_i, scale) \quad (1)$$

where $scale = \max(|x_1|, \dots, |x_n|)$ is the scaling factor. $Q_m(\cdot, scale)$ quantizes the given element with the scaling factor $scale$ and the number of mantissa bits m . The exact form of Q_m depends on the numerical format and can be found in Appendix J. For instance, INT m quantization transformation is defined as follows:

$$Q_m(x_i, scale) = s \cdot \left\lfloor \frac{x_i}{s} \right\rfloor, \text{ where } s = \frac{scale}{2^{m-1} - 1}, \text{ and } \lfloor \cdot \rfloor \text{ is the rounding to the nearest integer.} \quad (2)$$

Definition 3.2 (Magnitude-based sparsity). Let $\mathbf{x} \in \mathbb{R}^n$ be a block of n numbers. We assume n is divisible by M and we consider each group of M elements in the block. The magnitude-based N:M sparsity transformation can be formulated as:

$$\tilde{x}_i := \begin{cases} 0 & \text{if } |x_i| < \xi \\ x_i & \text{otherwise} \end{cases}, \text{ for } i = 1, 2, \dots, M \quad (3)$$

where ξ is the N -th largest element in $\mathbf{x} = \{|x_1|, \dots, |x_M|\}$. The same formula can be adjusted to represent $p\%$ unstructured sparsity by defining ξ as the N -th largest element in the tensor, where $N = \lceil M \cdot p/100 \rceil$, M is the number of elements in the tensor, and $\lceil \cdot \rceil$ is the operation of rounding to the nearest integer.

In the remaining of this section, we delve into the composition of quantization and sparsity at two different levels. First, we examine the effects of applying this composition in different orders at the tensor level, observing how individual tensors are altered. Then, we explore how the composition influences the result of the dot product operation.

3.1 Tensor-level analysis

Quantization and sparsity transformations inherently introduce errors by decreasing precision or pruning tensor elements. To study the composition of quantization and sparsity transformations at the tensor level, we introduce formal definitions of transformation error and orthogonality. We prove that orthogonality between sparsity and quantization *does not* persist within this composition. The following definition formalizes the error for a specific transformation at the block level, which consists of a subset of tensor elements.

Definition 3.3 (Transformation error). Let $\mathbf{x} \in \mathbb{R}^n$ be a block of n numbers, which are the input of a transformation $f : \mathbb{R}^n \rightarrow \mathbb{R}^n$. We define $\varepsilon_f(\mathbf{x}) := \mathbf{x} - f(\mathbf{x})$ as the error of the transformation f .

Definition 3.3 can be extended to the tensor level, despite being defined at the block level. The cumulative error of a tensor can be viewed as the summation of individual errors across all its constituent blocks. Hence, the theorems analyzed at the block level are indicative of the behavior when scaled up to the tensor level.

Combining two compression methods (transformations) is expected to introduce additional error. Any error introduced by the first transformation becomes part of the input to the second transformation, potentially amplifying the initial error and resulting in a larger overall error.

Definition 3.4 (Tensor-level orthogonality). We define two transformations f and g to be *orthogonal* if any order of their composition does not introduce any additional error, and thus, the following inequalities hold:

$$\forall \mathbf{x} \in \mathbb{R}^n, \quad \|\varepsilon_{g \circ f}(\mathbf{x})\| \leq \|\varepsilon_f(\mathbf{x})\| + \|\varepsilon_g(\mathbf{x})\| \wedge \|\varepsilon_{f \circ g}(\mathbf{x})\| \leq \|\varepsilon_f(\mathbf{x})\| + \|\varepsilon_g(\mathbf{x})\| \quad (4)$$

Theorem 3.5. Let q be the max-scaled block-wise quantization and s be the magnitude-based sparsity transformation. Applying sparsity before quantization does not introduce additional error:

$$\forall \mathbf{x} \in \mathbb{R}^n, \quad \|\varepsilon_{q \circ s}(\mathbf{x})\| \leq \|\varepsilon_q(\mathbf{x})\| + \|\varepsilon_s(\mathbf{x})\| \quad (5)$$

Moreover, the equality is attainable.

Proof. Let n_s represent the number of elements pruned from the block by the sparsity transformation. Without loss of generality, we assume that the last n_s elements in the block are pruned, as permuting the elements does not affect the block's norm. Since the sparsity transformation does not prune the largest element in the block, the *scale* parameter of quantization remains unchanged. Consequently, the quantization error for the non-zero components before and after sparsity remains the same:

$$\|\varepsilon_{q \circ s}(\mathbf{x})\| = \left\| \begin{pmatrix} x_1 \\ \vdots \\ x_{n-n_s} \\ x_{n-n_s+1} \\ \vdots \\ x_n \end{pmatrix} - q \begin{pmatrix} x_1 \\ \vdots \\ x_{n-n_s} \\ 0 \\ \vdots \\ 0 \end{pmatrix} \right\| = \left\| \begin{pmatrix} \varepsilon_q(\mathbf{x})_1 \\ \vdots \\ \varepsilon_q(\mathbf{x})_{n-n_s} \\ x_{n-n_s+1} \\ \vdots \\ x_n \end{pmatrix} \right\| \leq \left\| \begin{pmatrix} \varepsilon_q(\mathbf{x})_1 \\ \vdots \\ \varepsilon_q(\mathbf{x})_{n-n_s} \\ 0 \\ \vdots \\ 0 \end{pmatrix} \right\| + \quad (6)$$

$$+ \left\| \begin{pmatrix} 0 \\ \vdots \\ 0 \\ x_{n-n_s+1} \\ \vdots \\ x_n \end{pmatrix} \right\| \leq \left\| \begin{pmatrix} \varepsilon_q(\mathbf{x})_1 \\ \vdots \\ \varepsilon_q(\mathbf{x})_{n-n_s} \\ \varepsilon_q(\mathbf{x})_{n-n_s+1} \\ \vdots \\ \varepsilon_q(\mathbf{x})_n \end{pmatrix} \right\| + \left\| \begin{pmatrix} \varepsilon_s(\mathbf{x})_1 \\ \vdots \\ \varepsilon_s(\mathbf{x})_{n-n_s} \\ \varepsilon_s(\mathbf{x})_{n-n_s+1} \\ \vdots \\ \varepsilon_s(\mathbf{x})_n \end{pmatrix} \right\| = \|\varepsilon_s(\mathbf{x})\| + \|\varepsilon_q(\mathbf{x})\| \quad (7)$$

To demonstrate that equality is attainable, we consider the block of floating-point numbers $\mathbf{x} = (4.0, 4.1)^T$, INT4 quantization and 1 : 2 sparsity.

$$s(\mathbf{x}) = \begin{pmatrix} 0.0 \\ 4.1 \end{pmatrix} \quad q(\mathbf{x}) = \begin{pmatrix} 4.0 \\ 4.0 \end{pmatrix} \quad q(s(\mathbf{x})) = \begin{pmatrix} 0.0 \\ 4.0 \end{pmatrix} \quad (8)$$

The L1-norms of the transformation errors are the following:

$$\|\varepsilon_s(\mathbf{x})\|_1 = \left\| \begin{pmatrix} 4.0 \\ 0.0 \end{pmatrix} \right\|_1 = 4.0 \quad \|\varepsilon_q(\mathbf{x})\|_1 = \left\| \begin{pmatrix} 0.0 \\ 0.1 \end{pmatrix} \right\|_1 = 0.1 \quad \|\varepsilon_{q \circ s}(\mathbf{x})\|_1 = \left\| \begin{pmatrix} 4.0 \\ 0.1 \end{pmatrix} \right\|_1 = 4.1 \quad (9)$$

Therefore, $\|\varepsilon_{q \circ s}(\mathbf{x})\|_1 = \|\varepsilon_q(\mathbf{x})\|_1 + \|\varepsilon_s(\mathbf{x})\|_1$ is attainable. \square

Theorem 3.6. Let q be the max-scaled block-wise quantization and s be the magnitude-based sparsity transformation. Applying quantization before sparsity *may* introduce additional error:

$$\exists \mathbf{x} \in \mathbb{R}^n, \quad \|\varepsilon_{s \circ q}(\mathbf{x})\| > \|\varepsilon_q(\mathbf{x})\| + \|\varepsilon_s(\mathbf{x})\| \quad (10)$$

Proof. Consider the block of floating-point numbers $\mathbf{x} = (3.9, 4.0)^T$, INT4 quantization q and 1:2 sparsity s . After applying the quantization transformation to the block, initial relation between its elements $x_i < x_j$ is no longer preserved and both elements have equal probability to be zeroed out by the sparsity transformation. If sparsity zeroes out the element that was initially larger, the resulting error can exceed the sum of the errors caused by each transformation individually:

$$s(\mathbf{x}) = \begin{pmatrix} 0.0 \\ 4.0 \end{pmatrix} \quad q(\mathbf{x}) = \begin{pmatrix} 4.0 \\ 4.0 \end{pmatrix} \quad s(q(\mathbf{x})) = \begin{pmatrix} 4.0 \\ 0.0 \end{pmatrix} \quad (11)$$

$$\|\varepsilon_s(\mathbf{x})\| = \left\| \begin{pmatrix} 3.9 \\ 0.0 \end{pmatrix} \right\|_1 = 3.9 \quad \|\varepsilon_q(\mathbf{x})\| = \left\| \begin{pmatrix} -0.1 \\ 0.0 \end{pmatrix} \right\| = 0.1 \quad \|\varepsilon_{q \circ s}(\mathbf{x})\|_1 = \left\| \begin{pmatrix} -0.1 \\ 4.0 \end{pmatrix} \right\|_1 = 4.1 \quad (12)$$

Thus, for this particular input \mathbf{x} , the inequality $\|\varepsilon_{q \circ s}(\mathbf{x})\|_1 > \|\varepsilon_q(\mathbf{x})\|_1 + \|\varepsilon_s(\mathbf{x})\|_1$ holds true. \square

Moreover, a global upper bound exists for the additional error arising from this specific order of transformations (quantization \rightarrow sparsity). This upper bound is solely determined by the quantization method and the parameters of the sparsity scheme, independent of the input data. The following theorem precisely quantifies the magnitude of this additional error.

Theorem 3.7. Let q be the max-scaled block-wise quantization and s be the magnitude-based N:M sparsity transformation. Let $step$ be the least upper bound for the magnitude of the quantization error for one element: $step = \sup\{|\varepsilon_q(\mathbf{x})_i| \mid \mathbf{x} \in \mathbb{R}^n, i \in \{1 \dots n\}\}$. Then the error of the composition $s \circ q$ with respect to L_1 norm has the following upper bound:

$$\forall \mathbf{x} \in \mathbb{R}^n, \|\varepsilon_{s \circ q}(\mathbf{x})\|_1 \leq \|\varepsilon_q(\mathbf{x})\|_1 + \|\varepsilon_s(\mathbf{x})\|_1 + \underbrace{2 \cdot step \cdot \frac{M - N}{M} \cdot n}_{\text{additional error}} \quad (13)$$

Proof of Theorem 3.7 can be found in Appendix I. As a corollary of Theorem 3.5, 3.6, and 3.7, it follows that the optimal order of transformations is sparsity followed by quantization, as this sequence *does not* introduce any additional error. Moreover, according to Definition 3.4, quantization and sparsity are *not* orthogonal at the tensor level.

3.2 Orthogonality of dot product operation

In this section, we delve into the error linked with the dot product operation, which is the primary operation in DNNs. Our analysis focuses on scenarios where weight tensors undergo sparsification and quantization, while activation tensors solely undergo quantization. We first extend the definition of transformation error to the dot product level.

Definition 3.8 (Transformation error over the dot product). Let $\mathbf{x}, \mathbf{w} \in \mathbb{R}^n$ denote the inputs of a transformation $f : \mathbb{R}^n \rightarrow \mathbb{R}^n$ and the dot product operation $\langle \cdot, \cdot \rangle : \mathbb{R}^n \times \mathbb{R}^n \rightarrow \mathbb{R}$. We define $\varepsilon_f^D(\mathbf{x}, \mathbf{w}) := \langle \mathbf{x}, \mathbf{w} \rangle - \langle f(\mathbf{x}), f(\mathbf{w}) \rangle$ as the error of the transformation f over dot product. Similarly, we define $\varepsilon_{f,g}^D(\mathbf{x}, \mathbf{w}) := \langle \mathbf{x}, \mathbf{w} \rangle - \langle f(\mathbf{x}), g(\mathbf{w}) \rangle$ as the error over the dot product when different transformations are applied to x and w .

At the dot product level, we define two compression methods as *orthogonal* if any order of their composition does not introduce additional error, akin to Definition 3.4. In the following theorem, we demonstrate that any combination of sparsity and quantization yields additional error, rendering these two methods non-orthogonal.

Theorem 3.9. Let q be the max-scaled block-wise quantization, s be the magnitude-based sparsity transformation, c be the composition which is either $s \circ q$ or $q \circ s$ and I be the identity function. Max-scaled quantization q and sparsity s produce additional error in any order, given that only the second operand, i.e., weight, is sparsified:

$$\exists \mathbf{x}, \mathbf{w} \in \mathbb{R}^n, |\varepsilon_{q,c}^D(\mathbf{x}, \mathbf{w})| > |\varepsilon_{I,s}^D(\mathbf{x}, \mathbf{w})| + |\varepsilon_q^D(\mathbf{x}, \mathbf{w})| \quad (14)$$

Moreover,

$$|\varepsilon_{q,c}^D(\mathbf{x}, \mathbf{w})| \leq |\varepsilon_{I,s}^D(\mathbf{x}, \mathbf{w})| + |\varepsilon_q^D(\mathbf{x}, \mathbf{w})| + \underbrace{|\langle q(\mathbf{x}), \tilde{\varepsilon}_c(\mathbf{w}) \rangle| + |\langle \varepsilon_q(\mathbf{x}), \varepsilon_s(\mathbf{w}) \rangle|}_{\text{additional error}} \quad (15)$$

where $\tilde{\varepsilon}_c(\mathbf{x})$ is the correction error vector of the composition:

$$\varepsilon_c(\mathbf{x}) = \varepsilon_q(\mathbf{x}) + \varepsilon_s(\mathbf{x}) + \tilde{\varepsilon}_c(\mathbf{x}) \quad (16)$$

Proof. Error of the composition can be written as the following:

$$\varepsilon_{q,c}^D(\mathbf{x}, \mathbf{w}) = \langle \mathbf{x}, \mathbf{w} \rangle - \langle q(\mathbf{x}), c(\mathbf{w}) \rangle \quad (17)$$

$$= \langle \mathbf{x}, \mathbf{w} \rangle - \langle \mathbf{x} - \varepsilon_q(\mathbf{x}), \mathbf{w} - \varepsilon_c(\mathbf{w}) \rangle \quad (18)$$

$$= \langle \varepsilon_q(\mathbf{x}), \mathbf{w} \rangle + \langle \mathbf{x}, \varepsilon_c(\mathbf{w}) \rangle - \langle \varepsilon_q(\mathbf{x}), \varepsilon_c(\mathbf{w}) \rangle \quad (19)$$

$$= \langle \varepsilon_q(\mathbf{x}), \mathbf{w} \rangle + \langle \mathbf{x}, \varepsilon_q(\mathbf{w}) + \varepsilon_s(\mathbf{w}) + \tilde{\varepsilon}_c(\mathbf{w}) \rangle - \langle \varepsilon_q(\mathbf{x}), \varepsilon_q(\mathbf{w}) + \varepsilon_s(\mathbf{w}) + \tilde{\varepsilon}_c(\mathbf{w}) \rangle \quad (20)$$

$$= \underbrace{\langle \mathbf{x}, \varepsilon_s(\mathbf{w}) \rangle}_{\varepsilon_{I,s}^D(\mathbf{x}, \mathbf{w})} + \underbrace{\langle \mathbf{x}, \varepsilon_q(\mathbf{w}) \rangle + \langle \varepsilon_q(\mathbf{x}), \mathbf{w} \rangle - \langle \varepsilon_q(\mathbf{x}), \varepsilon_q(\mathbf{w}) \rangle}_{\varepsilon_q^D(\mathbf{x}, \mathbf{w})} + \underbrace{\langle \mathbf{x} - \varepsilon_q(\mathbf{x}), \tilde{\varepsilon}_c(\mathbf{w}) \rangle}_{q(\mathbf{x})} \quad (21)$$

$$- \langle \varepsilon_q(\mathbf{w}), \varepsilon_s(\mathbf{w}) \rangle \quad (22)$$

$$= \varepsilon_{I,s}^D(\mathbf{x}, \mathbf{w}) + \varepsilon_q^D(\mathbf{x}, \mathbf{w}) + \langle q(\mathbf{x}), \tilde{\varepsilon}_c(\mathbf{w}) \rangle - \langle \varepsilon_q(\mathbf{x}), \varepsilon_s(\mathbf{w}) \rangle \quad (23)$$

After adding the norms, we obtain the following:

$$|\varepsilon_{q,c}^D(\mathbf{x}, \mathbf{w})| \leq |\varepsilon_{I,s}^D(\mathbf{x}, \mathbf{w})| + |\varepsilon_q^D(\mathbf{x}, \mathbf{w})| + \underbrace{|\langle q(\mathbf{x}), \tilde{\varepsilon}_c(\mathbf{w}) \rangle|}_{\varepsilon_t} + \underbrace{|\langle \varepsilon_q(\mathbf{x}), \varepsilon_s(\mathbf{w}) \rangle|}_{\varepsilon_i} \quad (24)$$

where ε_t and ε_i are the additional error terms.

To prove non-orthogonality, consider the blocks of floating-point numbers $x = (1.0, 1.0)^T$ and $w = (0.6, 1.3)^T$, HBF4 quantization q and 1:2 sparsity s . For these particular values of \mathbf{x} and \mathbf{w} , the inequality: $|\varepsilon_{q,c}^D(\mathbf{x}, \mathbf{w})| > |\varepsilon_q^D(\mathbf{x}, \mathbf{w})| + |\varepsilon_{I,s}^D(\mathbf{x}, \mathbf{w})|$ holds true. The exact calculations can be found in Appendix I. \square

Analysis of the additional error. As a corollary of Theorem 3.9, the combination of max-scaled quantization and sparsity is *not* orthogonal, resulting in two additional error terms.

The term ε_t encompasses the correction vector of the composition $\tilde{\varepsilon}_c$, which propagates the error from the tensor level to the dot product level. Depending on the order of the composition the value of ε_t varies.

If sparsity precedes quantization, the correction vector $\tilde{\varepsilon}_{q \circ s}(\mathbf{w})$ exclusively comprises negative quantization errors for the elements pruned by the sparsity transformation:

$$\tilde{\varepsilon}_{q \circ s}(\mathbf{w})_i = \begin{cases} -\varepsilon_q(\mathbf{w})_i, & s(\mathbf{x})_i = 0 \\ 0, & \text{otherwise} \end{cases} \quad (25)$$

However, if quantization is applied first, certain elements in the block may become equal, resulting in the sparsity removing a different set of elements. Formally, if w_i is pruned by s but not by $s \circ q$, there exists a w_j , where $j \neq i$, such that $q(\mathbf{w})_i = q(\mathbf{w})_j$. In this scenario, $\tilde{\varepsilon}_{s \circ q}(\mathbf{w})_i = -\varepsilon_s(\mathbf{w})_i$ and $\tilde{\varepsilon}_{s \circ q}(\mathbf{w})_j = \varepsilon_s(\mathbf{w})_j - \varepsilon_q(\mathbf{w})_j$. Otherwise, it only contains the quantization errors of the pruned elements. Therefore, the magnitude of the correction vector for the composition $s \circ q$ is generally larger than that of the reverse order. Apart from the quantization errors, the correction vector also contains pruned elements, which are larger by orders of magnitude except in a few improbable edge cases. This results in the overall value of ε_t being larger, implying that *the order of applying sparsity first and then quantization is optimal for dot product*.

The term ε_i also contributes to the additional error, encoding the interaction between the error vectors $\varepsilon_q(\mathbf{x})$ and $\varepsilon_s(\mathbf{w})$. However, ε_i is less significant than ε_t , as it contains the quantization error, the norm of which is generally orders of magnitude lower than the norm of the original block. In addition, ε_i contains the sparsity error, which involves the smallest weights, diminishing the significance of this additional error.

Finally, to experimentally validate our theoretical findings, we define orthogonality bound to assess whether the transformations are orthogonal.

Definition 3.10 (Orthogonality bound). Let M be a DNN model under consideration, $\text{EM}(M)$ be an evaluation metric that measures the performance of the model M (e.g. Perplexity or Cross-Entropy Loss), $\text{EM}_C(M)$ be the evaluation metric of the model M with transformation C , which is either sparsity S or quantization Q . Moreover, let $\text{Err}_C(M) = \text{EM}_C(M) - \text{EM}(M)$ be the evaluation metric error of the transformation C for the model M . We define *orthogonality bound* as:

$$\text{Orthogonality Bound} = \text{EM}(M) + \text{Err}_Q(M) + \text{Err}_S(M) \quad (26)$$

Table 1: Perplexities of OPT-125M and LLaMA-2-7B on WikiText2 for combinations of different number formats and sparsity types, considering both orders of compression operations. “50%” denotes unstructured sparsity, while “2:4” represents a variant of N:M structured sparsity. In the FP32 columns, only one perplexity for each compression order is reported because no quantization is applied. The best results for each (sparsity type, number format) pair are highlighted in bold.

Sparsity type	Order	OPT-125M						LLaMA-2-7B					
		FP32	INT8	MXFP8	MXFP6	HBFP8	HBFP6	FP32	INT8	MXFP8	MXFP6	HBFP8	HBFP6
0% (Dense)	-	27.65	28.06	28.45	28.01	27.81	29.91	5.12	5.15	5.17	5.16	5.12	5.24
50%	S→Q	29.94	30.22	31.13	31.20	30.46	32.51	6.31	6.94	6.40	6.38	6.32	6.51
	Q→S	-	34.71	36.39	35.60	37.48	40.86	-	8.13	8.47	9.32	9.86	10.20
2:4	S→Q	31.89	32.76	33.99	33.41	32.25	34.58	9.30	9.37	9.35	9.32	9.39	10.68
	Q→S	-	45.06	44.16	42.25	46.57	55.64	-	14.65	14.35	14.50	14.98	18.64

If the compression methods are not orthogonal, and the evaluation metric indicates better model performance with lower values, we expect the compressed model’s evaluation metric to exceed the orthogonality bound.

4 Experimental methodology and results

Models, datasets, and evaluation setup. We study the most widely adopted Transformer-based models, including OPT [69] and LLaMA [58] model families. In line with prior work [64, 15, 53], we fine-tune pretrained models and evaluate perplexity on the WikiText2 [36] dataset. In addition, we assess orthogonality across different metrics of ViT [10] on ImageNet-1k [7]. In all experiments, we designate the dense FP32 configuration as our primary baseline. Our experiments span a diverse range of configurations to validate our theoretical findings, including various variants of max-scaled formats, such as INT8 quantization with per channel scaling [8], HBFP8/6 [11], and MXFP8/6 [50]. We primarily study magnitude-based 50% unstructured and 2:4 structured sparsity with sparsity-aware fine-tuning. We evaluate the impact of increased compression on ViT-B/16 by applying 75% unstructured sparsity, 1:4 structured sparsity, and HBFP4. Detailed results can be found in Appendix F. We also explore post-training one-shot sparsity methods like SparseGPT [15] and Wanda [53] in Appendix E. In our experiments, we evaluate the impact of each compression method by analyzing the variations in perplexity and cross-entropy loss compared to the baseline, thereby focusing on the cumulative error in the final model output. Additionally, we analyze the errors of intermediate layers to support our mathematical analysis, as detailed in Appendix G. Note that we focus on cross-entropy loss for ViT-B/16 instead of classification accuracy. This is because accuracy remains unaffected as long as the most likely label remains unchanged, regardless of its absolute value. However, our primary metric for orthogonality bound is the aggregated errors introduced in the final model output distribution. Table 7 in Appendix F evaluates orthogonality bound on additional metrics.

Experimental setup. We exclusively sparsify and/or quantize layers with trainable parameters. Specifically, we target all linear layers in LLMs, and all linear and convolution layers (including the initial embedding layer) in ViT-B/16. These layers collectively constitute approximately 99% of the total parameters. In all experiments, we sparsify weights while keeping activation dense. Both weights and activation tensors are quantized before matrix multiplication operations. For OPT, LLaMA, and ViT fine-tuning, we employ sparse fine-tuning on a dense FP32 pre-trained model, recomputing sparsity masks at each iteration. In experiments involving sparsity followed by quantization (S→Q), we apply one-shot quantization to sparse fine-tuned models. Conversely, for experiments with the reverse order (Q→S), we directly fine-tune the model in a quantized and sparsified manner. At each iteration, we quantized activations and weights while applying sparsity to weight tensors. We validate the effectiveness of these compression recipes through an ablation study, the details of which are presented in Appendix D. To ensure fair comparison, we maintain uniform hyperparameters across various number formats for a given model and sparsity type (details in Appendix B). We present a limited sensitivity study on the initial seed number in Table 8 in Appendix H.

Table 2: OPT-125M, OPT-6.7B, LLaMA-2-7B, and LLaMA-3-8B perplexities on WikiText2 and ViT-B/16 CE loss on ImageNet-1k for the combination of various number formats and sparsity types.

Sparsity type	Number format	OPT-125M		OPT-6.7B		LLaMA-2-7B		LLaMA-3-8B		ViT-B/16	
		PPL↓	Orth. bound	PPL↓	Orth. bound	PPL↓	Orth. bound	PPL↓	Orth. bound	CE Loss↓	Orth. bound
0%	FP32	27.65	-	10.86	-	5.12	-	5.53	-	0.703	-
	INT8	28.06	-	10.95	-	5.19	-	5.63	-	0.706	-
	MXFP8	28.45	-	11.25	-	5.17	-	5.62	-	0.722	-
	MXFP6	28.01	-	11.02	-	5.16	-	5.62	-	0.715	-
	HBFP8	27.81	-	10.88	-	5.12	-	5.56	-	0.704	-
	HBFP6	29.91	-	11.20	-	5.24	-	5.87	-	0.718	-
50%	FP32	29.94	-	11.30	-	6.31	-	10.09	-	0.723	-
	INT8	30.22	30.35	11.37	11.39	6.94	6.38	10.85	10.19	0.728	0.725
	MXFP8	31.13	30.74	11.74	11.69	6.40	6.36	10.34	10.18	0.745	0.742
	MXFP6	31.20	30.30	11.53	11.44	6.38	6.35	10.15	10.18	0.734	0.735
	HBFP8	30.46	30.18	11.31	11.32	6.32	6.31	10.12	10.12	0.724	0.723
	HBFP6	32.51	32.2	11.94	11.65	6.51	6.43	10.55	10.43	0.736	0.737
2:4	FP32	31.89	-	15.48	-	9.30	-	13.07	-	0.759	-
	INT8	32.76	32.30	15.61	15.57	9.37	9.37	13.23	13.17	0.762	0.761
	MXFP8	33.99	32.69	15.70	15.87	9.35	9.35	13.35	13.16	0.781	0.777
	MXFP6	33.41	32.25	15.95	15.64	9.32	9.34	13.2	13.16	0.770	0.771
	HBFP8	32.25	32.05	15.57	15.50	9.39	9.31	13.11	13.1	0.760	0.759
	HBFP6	34.58	34.15	16.98	15.82	10.68	9.42	13.64	13.41	0.774	0.773

4.1 Empirical study 1: Order of sparsity and quantization

This section presents empirical evidence demonstrating that applying sparsity before quantization leads to better perplexities compared to the reverse order. These results align with the theoretical arguments in Section 3.1. Table 1 presents perplexities for OPT-125M and LLaMA-2-7B under various number formats and sparsity types. We compare the order of operations across different configurations: sparsity followed by quantization (S→Q) and quantization followed by sparsity (Q→S). Configurations with lower perplexities are highlighted in bold. Consistently, we observe that the S→Q order yields better perplexities across all number formats for magnitude-based sparsity. As discussed in Section 3.1, in the case of Q→S, quantizing a tensor can alter the order of its elements due to changes in magnitudes. If magnitude-based sparsity removes elements of the quantized tensor that were originally larger before quantization, the error of the composition may exceed the sum of the errors caused by each transformation individually. This compounded error further propagates through subsequent dot-product and vector operations, impacting overall model performance.

4.2 Empirical study 2: Non-Orthogonality between sparsity and quantization

This section demonstrates that combining sparsity and quantization results in additional error, surpassing the sum of their individual errors. Table 2 presents perplexities for OPT-125M, OPT-6.7B, LLaMA-2-7B and LLaMA-3-8B on WikiText2, and cross-entropy (CE) loss for ViT-B/16 on ImageNet-1k for various combinations of number formats and sparsity schemes. Following our conclusions regarding the order of operations, we only report results for S→Q. We compute the orthogonality bound for each combination by summing the individual errors from quantization and sparsity relative to the baseline dense FP32 model, using Equation 26. Each model’s performance is compared against this bound, with superior results highlighted in bold. In the majority of configurations, perplexity and cross-entropy loss values exceed the orthogonality bounds, validating the non-orthogonality of sparsity and quantization.

We mathematically show (Section 3.2) that the additional error introduced by combining sparsity and quantization significantly depends on the values of quantized activation tensors and the quantization error of sparsified weights. This error tends to amplify through successive dot products and vector operations. Consequently, the quantization error affects the additional error caused by the composition more than the sparsification error. The gap between the model’s performance and the orthogonality bound is minimal for number formats with minimal performance decrease, whereas larger errors are observed for formats with larger errors. For instance, HBFP6 results in a 2.26 increase in perplexity for OPT-125M, while its combination with 50% unstructured sparsity leads to a 4.86 increase.

Our analysis reveals that both model size and compression ratio significantly influence the additional error introduced by combining sparsity and quantization. Larger models exhibit greater tolerance to these compression methods, resulting in lower additional errors. Moreover, formats with mini-

mal quantization errors (e.g. MXFP8), and sparsity types with minimal sparsification errors (e.g. unstructured sparsity) lead to lower additional errors, even for smaller models. The effect of high quantization error is more pronounced for sparsity schemes known for higher errors. For instance, HBFP6’s combination with 2:4 sparsity causes a 6.93 perplexity increase for OPT-125M and a 6.12 perplexity increase for OPT-6.7B. In contrast, combining HBFP6 with unstructured sparsity results in smaller increases of 4.86 and 0.79 for the respective models.

We also observe instances where the orthogonality bound is slightly higher than the actual perplexity: (a) INT8 with 50% unstructured sparsity for both OPT models, (b) MXFP8 with 2:4 sparsity for OPT-6.7B, (c) MXFP6 with 2:4 sparsity for LLaMA-2-7B, and (d) MXFP6 50% unstructured sparsity for LLaMa-3-8B. Although these occurrences do not consistently correlate with specific formats, sparsity types, or model sizes, they do not contradict our theoretical analysis, which primarily concerns upper bounds of errors and does not entirely rule out orthogonal cases. Furthermore, orthogonal configurations still result in larger errors compared to applying either sparsity or quantization alone. Our mathematical analysis (Theorem 3.9) indicates that there *exists at least one occurrence* where the orthogonality is *not* preserved. This underscores the need for careful examination when applying these compression methods together, as they do not guarantee high accuracies. Delving into cases where orthogonality is preserved falls beyond the scope of this paper and we leave it for future work.

We also observe that although the cross-entropy loss for ViT-B/16 is higher than the calculated orthogonality bound in most cases in Table 2, the difference is relatively small. We hypothesize the reason behind this behavior is due to the fact that ViT-B/16 being a vision model that operates on images is more robust to quantization and sparsity errors than LLMs that operate on text. Hence, the quantization and sparsity levels shown in Table 2 are not sufficient to induce large errors, and hide the non-orthogonality of quantization and sparsity. To test our hypothesis, we increase the compression further by employing 75% unstructured sparsity, 1:4 structured sparsity and HBFP4 on ViT-B/16 (Appendix F). The results show that the difference between the baseline cross-entropy loss and the calculated orthogonality bound for these cases increases significantly validating the non-orthogonality of quantization and sparsity. This increase in cross-entropy loss translates to a significant non-orthogonal drop in accuracy as well.

5 Discussion

Our theoretical analysis and experimental results offer multiple insights for ML model practitioners. First, our analysis demonstrates a risk-free method to improve model performance, measured by lower perplexity and/or higher accuracy, through choosing the optimal ordering of compression operations for any max-scaled number format and magnitude-based pruning scheme. This contribution is particularly important in the current ML landscape, where sparsity and quantization are pivotal methods for reducing the memory footprint and bandwidth requirements of state-of-the-art LLMs. Second, we show that calculating the orthogonality bound offers a close enough estimate of model performance (e.g., accuracy, perplexity, etc.) under conditions of quantization and sparsity. This bound can streamline the search for optimal sparse-quantized model configurations by effectively narrowing the search space. There is an inherent tradeoff between the hardware benefits of various sparse-quantized configurations and the achieved model performance. Quantization bit-width and sparsity level are key factors influencing the memory and bandwidth requirements for serving these models. For example, at a 50% sparsity level, 8-bit and 6-bit quantization result in total reductions in memory footprint and bandwidth requirements by $8\times$ and $10.7\times$, respectively.

Ideally, practitioners aim to maximize compression (increase sparsity ratio and/or reduce quantization effective bitwidth). Our analysis elucidates the individual and combined impacts of these factors across a range of recent large models, providing practical guidelines to achieve the highest compression without compromising model performance. Typically, 8-bit quantization with any max-scaled number format can serve as a direct replacement for FP32 when combined with any form of sparsity in the optimal order (S→Q). As discussed in Section 4, certain models exhibit sensitivity to sub-8bit number formats and structured sparsity combinations, even when applied in an optimal order. In scenarios where improvements in arithmetic density (TOPS/mm²) and memory footprint justify a slight reduction in model performance, such as the deployment of large models on edge devices, these combinations may still be viable.

In this work, we do not consider heterogeneous sparsity and quantization schemes, where the sparsity fraction and quantization bit-width vary across layers and differ between activation and weight tensors. Such approaches [50, 35, 20, 12] have demonstrated to be effective in maintaining model accuracy or perplexity while improving compressing ratio. However, these schemes may not be hardware-friendly, introduce noticeable overhead, and are impractical to implement on off-the-shelf hardware platforms (e.g., GPU, TPU). We leave the investigation of the interactions between these heterogeneous quantization and sparsity schemes for future work.

6 Conclusion

We provide a comprehensive analysis of the interplay between quantization and sparsity in DNNs, showing that applying sparsity before quantization ($S \rightarrow Q$) minimizes additional errors and yields better model accuracy. Moreover, our mathematical analysis and extensive empirical study with large language models (OPT, LLaMA) and vision transformers (ViT) demonstrate that quantization and sparsity are *not* orthogonal and their combined use can adversely affect model accuracy. Our findings provide valuable insights for optimizing the compression of large models while preserving accuracy.

Acknowledgments and Disclosure of Funding

We extend our gratitude towards Zhifeng Chen, Cliff Young, James Laudon, and Shashwat Shrivastava for reviewing the paper and providing insightful feedback. We also thank the extended team at Google DeepMind, who enabled and supported this research direction. This work was partially supported by the SNSF project “Unified Accelerators for Post-Moore Machine Learning” (200021_212757) and a Microsoft Research PhD Fellowship.

References

- [1] E. Almazrouei, H. Alobeidli, A. Alshamsi, A. Cappelli, R. Cojocaru, M. Debbah, Étienne Goffinet, D. Hesslow, J. Launay, Q. Malartic, D. Mazzotta, B. Noune, B. Pannier, and G. Penedo. The Falcon Series of Open Language Models. *arXiv*, 2023.
- [2] A. R. Bambhaniya, A. Yazdanbakhsh, S. Subramanian, et al. Progressive Gradient Flow for Robust N:M Sparsity Training in Transformers. *arXiv*, 2024.
- [3] T. B. Brown, B. Mann, N. Ryder, et al. Language Models are Few-Shot Learners. In *NeurIPS*, 2020.
- [4] S. Dai, R. Venkatesan, M. Ren, et al. VS-Quant: Per-vector Scaled Quantization for Accurate Low-Precision Neural Network Inference. *MLSys*, 2021.
- [5] B. Darvish Rouhani, N. Garegrat, T. Savell, et al. OCP Microscaling (MX) Specification. *Open Compute Project*, 2023.
- [6] B. Darvish Rouhani, D. Lo, R. Zhao, et al. Pushing the Limits of Narrow Precision Inferencing at Cloud Scale with Microsoft Floating Point. In *NeurIPS*, 2020.
- [7] J. Deng, W. Dong, R. Socher, et al. ImageNet: A Large-scale Hierarchical Image Database. In *CVPR*, 2009.
- [8] T. Dettmers, M. Lewis, Y. Belkada, et al. LLM.int8(): 8-bit Matrix Multiplication for Transformers at Scale. In *NeurIPS*, 2022.
- [9] S. Ding, D. Qiu, D. Rim, et al. USM-Lite: Quantization and Sparsity Aware Fine-Tuning for Speech Recognition with Universal Speech Models. In *ICASSP*, 2023.
- [10] A. Dosovitskiy, L. Beyer, A. Kolesnikov, et al. An Image is Worth 16x16 Words: Transformers for Image Recognition at Scale. In *ICLR*, 2021.
- [11] M. Drumond, T. Lin, M. Jaggi, et al. Training DNNs with Hybrid Block Floating Point. *NeurIPS*, 2018.
- [12] U. Evci, T. Gale, J. Menick, et al. Rigging the Lottery: Making All Tickets Winners. In *ICML*, 2020.
- [13] J. Frankle and M. Carbin. The Lottery Ticket Hypothesis: Finding Sparse, Trainable Neural Networks. In *ICLR*, 2019.
- [14] E. Frantar and D. Alistarh. Optimal Brain Compression: A Framework for Accurate Post-Training Quantization and Pruning. *NeurIPS*, 2022.
- [15] E. Frantar and D. Alistarh. SparseGPT: Massive Language Models Can be Accurately Pruned in One-Shot. In *ICML*, 2023.
- [16] E. Frantar, C. Riquelme, N. Houlsby, et al. Scaling Laws for Sparsely-connected Foundation Models. In *ICLR*, 2024.
- [17] Y. Guo, A. Yao, and Y. Chen. Dynamic Network Surgery for Efficient DNNs. *NeurIPS*, 2016.
- [18] S. Han, H. Mao, and W. J. Dally. Deep Compression: Compressing Deep Neural Networks with Pruning, Trained Quantization and Huffman Coding. *arXiv preprint arXiv:1510.00149*, 2015.
- [19] S. Han, J. Pool, J. Tran, et al. Learning both Weights and Connections for Efficient Neural Network. *NeurIPS*, 2015.
- [20] S. B. Harma, A. Chakraborty, B. Falsafi, et al. Accuracy Boosters: Epoch-Driven Mixed-Mantissa Block Floating-Point for DNN Training. *arXiv preprint arXiv:2211.10737*, 2022.
- [21] B. Hassibi, D. G. Stork, and G. J. Wolff. Optimal Brain Surgeon and General Network Pruning. In *IEEE international conference on neural networks*, 1993.
- [22] B. Hawks, J. Duarte, N. J. Fraser, et al. Ps and qs: Quantization-aware pruning for efficient low latency neural network inference. *Frontiers in Artificial Intelligence*, 4:676564, 2021.
- [23] P. Hu, X. Peng, H. Zhu, et al. OPQ: Compressing Deep Neural Networks with One-shot Pruning-Quantization. In *AAAI*, 2021.
- [24] I. Hubara, B. Chmiel, M. Island, et al. Accelerated Sparse Neural Training: A Provable and Efficient Method to Find N:M Transposable Masks. In *NeurIPS*, 2021.
- [25] A. Q. Jiang, A. Sablayrolles, A. Mensch, et al. Mistral 7B. *CoRR*, abs/2310.06825, 2023.
- [26] H. Kang. Accelerator-Aware Pruning for Convolutional Neural Networks. *IEEE Trans. Circuits Syst. Video Technol.*, 30(7):2093–2103, 2020.
- [27] S.-C. Kao, A. Yazdanbakhsh, S. Subramanian, et al. Training Recipe for N:M Structured Sparsity with Decaying Pruning Mask. *arXiv preprint arXiv:2209.07617*, 2022.
- [28] E. Kurtic, D. Campos, T. Nguyen, et al. The Optimal BERT Surgeon: Scalable and Accurate Second-order Pruning for Large Language Models. *arXiv preprint arXiv:2203.07259*, 2022.

- [29] A. Kuzmin, M. Nagel, M. van Baalen, et al. Pruning vs Quantization: Which is Better? In *NeurIPS*, 2023.
- [30] M. Lasby, A. Golubeva, U. Evci, et al. Dynamic Sparse Training with Structured Sparsity. *arXiv preprint arXiv:2305.02299*, 2023.
- [31] Y. LeCun, J. Denker, and S. Solla. Optimal Brain Damage. *NeurIPS*, 1989.
- [32] Z. Li, E. Wallace, S. Shen, et al. Train Big, then Compress: Rethinking Model Size for Efficient Training and Inference of Transformers. In *ICML*, 2020.
- [33] Z. Liu, J. Wang, T. Dao, et al. Deja Vu: Contextual Sparsity for Efficient LLMs at Inference Time. In *ICML*, 2023.
- [34] Y. Lu, S. Agrawal, S. Subramanian, et al. STEP: Learning N:M Structured Sparsity Masks from Scratch with Precondition. In *ICML*, 2023.
- [35] S. Ma, H. Wang, L. Ma, et al. The Era of 1-bit LLMs: All Large Language Models are in 1.58 Bits. *arXiv*, 2024.
- [36] S. Merity, C. Xiong, J. Bradbury, et al. Pointer Sentinel Mixture Models. In *ICLR*, 2017.
- [37] T. Mesnard, C. Hardin, R. Dadashi, et al. Gemma: Open Models Based on Gemini Research and Technology. *arXiv*, 2024.
- [38] P. Micikevicius, S. Narang, J. Alben, et al. Mixed Precision Training. *arXiv*, 2018.
- [39] P. Micikevicius, S. Oberman, P. Dubey, et al. OCP 8-bit Floating Point Specification (OFP8). *Open Compute Project*, 2023.
- [40] P. Micikevicius, D. Stolic, N. Burgess, et al. FP8 Formats for Deep Learning. *arXiv*, 2022.
- [41] Microsoft. MicroXcaling: A Library for Microservices Autoscaling. <https://github.com/microsoft/microxcaling>, 2024.
- [42] A. K. Mishra, J. A. Latorre, J. Pool, et al. Accelerating Sparse Deep Neural Networks. *ArXiv*, abs/2104.08378, 2021.
- [43] Nvidia. Enabling next-generation AI workloads: Announcing TPU v5p and AI Hypercomputer. <https://cloud.google.com/blog/products/ai-machine-learning/introducing-cloud-tpu-v5p-and-ai-hypercomputer>.
- [44] Nvidia. NVIDIA Ampere Architecture Whitepaper. Technical report, NVIDIA, 2021.
- [45] Nvidia. NVIDIA H100 Tensor Core GPU Architecture. Technical report, NVIDIA, 2022.
- [46] OpenAI. GPT-4 Technical Report. *CoRR*, abs/2303.08774, 2023.
- [47] J.-H. Park, K.-M. Kim, and S. Lee. Quantized Sparse Training: A Unified Trainable Framework for Joint Pruning and Quantization in DNNs. *TECS*, 2022.
- [48] J. Pool and C. Yu. Channel Permutations for N: M Sparsity. In *NeurIPS*, 2021.
- [49] B. D. Rouhani, R. Zhao, V. Elango, et al. With Shared Microexponents, A Little Shifting Goes a Long Way. In *ISCA*, 2023.
- [50] B. D. Rouhani, R. Zhao, A. More, et al. Microscaling Data Formats for Deep Learning. *arXiv*, 2023.
- [51] V. Sanh, T. Wolf, and A. Rush. Movement Pruning: Adaptive Sparsity by Fine-tuning. *NeurIPS*, 2020.
- [52] T. L. Scao, A. Fan, C. Akiki, et al. BLOOM: A 176B-Parameter Open-Access Multilingual Language Model. *arXiv*, 2022.
- [53] M. Sun, Z. Liu, A. Bair, et al. A Simple and Effective Pruning Approach for Large Language Models. *arXiv*, 2023.
- [54] W. Sun, A. Zhou, S. Stuijk, et al. DominoSearch: Find Layer-wise Fine-grained N:M Sparse Schemes from Dense Neural Networks. In *NeurIPS*, 2021.
- [55] A. Syed, P. H. Guo, and V. Sundarapandiyam. Prune and Tune: Improving Efficient Pruning Techniques for Massive Language Models. In *The First Tiny Papers Track at ICLR*, 2023.
- [56] V. Sze, Y. Chen, T. Yang, et al. *Efficient Processing of Deep Neural Networks*. Synthesis Lectures on Computer Architecture. Morgan & Claypool Publishers, 2020.
- [57] G. Team, R. Anil, S. Borgeaud, J.-B. Alayrac, et al. Gemini: A Family of Highly Capable Multimodal Models. *arXiv*, 2024.
- [58] H. Touvron, L. Martin, K. Stone, et al. Llama 2: Open Foundation and Fine-Tuned Chat Models. *arXiv*, 2023.
- [59] M. van Baalen, A. Kuzmin, S. S. Nair, et al. FP8 versus INT8 for Efficient Deep Learning Inference. *arXiv*, 2023.
- [60] S. Wang and P. Kanwar. BFloat16: The Secret to High Performance on Cloud TPUs, 2019.

- [61] T. Wang, K. Wang, H. Cai, et al. APQ: Joint Search for Network Architecture, Pruning and Quantization Policy. In *CVPR*, 2020.
- [62] W. Wen, C. Wu, Y. Wang, et al. Learning Structured Sparsity in Deep Neural Networks. *NeurIPS*, 29, 2016.
- [63] X. Wu, C. Li, R. Y. Aminabadi, et al. Understanding INT4 Quantization for Transformer Models: Latency Speedup, Composability, and Failure Cases. *arXiv*, 2023.
- [64] G. Xiao, J. Lin, M. Seznec, et al. SmoothQuant: Accurate and Efficient Post-Training Quantization for Large Language Models. In *ICML*, 2023.
- [65] Z. Yao, S. Cao, W. Xiao, et al. Balanced Sparsity for Efficient DNN Inference on GPU. In *AAAI*, 2019.
- [66] T. Yeh, M. Sterner, Z. Lai, et al. Be Like Water: Adaptive Floating Point for Machine Learning. In *ICML*, 2022.
- [67] C. Yu, T. Chen, Z. Gan, et al. Boost Vision Transformer with GPU-friendly Sparsity and Quantization. In *CVPR*, 2023.
- [68] O. Zafrir, G. Boudoukh, P. Izsak, et al. Q8BERT: Quantized 8Bit BERT. In *Fifth Workshop on Energy Efficient Machine Learning and Cognitive Computing - NeurIPS Edition, EMC2@NeurIPS*, 2019.
- [69] S. Zhang, S. Roller, N. Goyal, et al. OPT: Open Pre-trained Transformer Language Models. *arXiv*, 2022.
- [70] S. Q. Zhang, B. McDanel, and H. Kung. FAST: DNN Training under Variable Precision Block Floating Point with Stochastic Rounding. In *HPCA*, 2022.
- [71] A. Zhou, Y. Ma, J. Zhu, et al. Learning N:M Fine-grained Structured Sparse Neural Networks From Scratch. In *ICLR*, 2021.

Appendix

Table of Contents

A Additional related work	14
B Hyperparameters	15
C Compute resources and runtime	15
D Fine-tuning strategies	15
E Post-training one-shot sparsity methods	16
F Orthogonality bound for ViT	16
G Layer-wise error analysis	17
H Robustness analysis	18
I Proofs for the mathematical analysis	18
J Definitions of Q for numerical formats	20
K Analysis of the upper bound of the dot product error	21
K.1 Upper bound is reachable	21
K.2 Contribution of additional error terms	22

1 A Additional related work

2 **Quantization.** Element-wise scaling formats, such as FP32, BFLOAT32 [60], and FP16 [38], consist of sign,
3 mantissa, and exponent components, differing in the bit allocation for each component. Conversely, block-wise
4 scaling formats assign scaling factors to blocks of elements, with block sizes varying by format. For instance,
5 INT8 employs per-tensor scaling, where a single scaling factor is shared by around 1K elements.

6 Recent research highlights the effectiveness of fine-grained block-wise scaling formats with block sizes smaller
7 than 100 elements, especially in the sub-8-bit regime for both training and inference [11, 49, 50, 70, 6]. These
8 formats are further categorized into single-level and two-level scaling. Single-level block-wise formats, such as
9 HBFP [11, 6] and MXINT [50], enable fixed-point arithmetic by sharing a single exponent within a block of
10 mantissa or integers. Two-level formats, like MXFP [49, 50, 40] and FP8, use more granular scaling factors at
11 the second level, offering greater robustness across diverse range of models.

12 **Sparsity.** Unstructured sparsity [18, 17, 13, 12] involves removing individual tensor elements without any
13 specific pattern. Structured sparsity [62], on the other hand, employs specific patterns when pruning tensor
14 elements. Recent work [65, 26] has highlighted the effectiveness of fine-grained N:M structured sparsity in
15 mitigating model accuracy loss. The introduction of the 2:4 structured-sparse Tensor Core in the Nvidia Ampere
16 architecture [44] has further driven research in developing N:M sparsity training recipes [42, 48, 71, 54, 24, 34].
17 The fundamental operation in any sparsification scheme is selecting candidate elements for pruning among which
18 magnitude-based sparsity [19] is one of the most widely used methods [34, 9, 2]. In addition, recent work has
19 introduced one-shot pruning methods, such as SparseGPT [15] and Wanda [53], aiming to eliminate the need for
20 an additional fine-tuning phase. While these methods achieve state-of-the-art performance for one-shot pruning,
21 evidence suggests that incorporating a fine-tuning phase can lead to better model quality [53, 55]. Although
22 these methods are proposed to eliminate fine-tuning and present state-of-the-art accuracies for one-shot pruning,
23 it has been shown that fine-tuning still improves accuracies significantly [53, 55].

Table 3: Types of max-scaled numerical encodings.

		Element-wise		Single-level block-wise			Two-level block-wise	
		FP32/FP16	BFloat16	INT	HBFP	MXINT	MXFP	FP8
Scaling level 1	Block size	1	1	1k	64	32	32	10k
	Scale type	HW	HW	SW	HW	HW	HW	SW
Scaling level 2	Block size	-	-	-	-	-	1	1
	Scale type	-	-	-	-	-	HW	HW

24 B Hyperparameters

25 We perform full parameter fine-tuning while applying magnitude-based sparsity methods. We find the optimal
 26 hyperparameters through grid search for each model and sparsity type and apply the same hyperparameters
 27 across all number formats, including FP32. We observe that fine-tuning in a Q→S order, where we quantize
 28 and sparsify tensors at each iteration, leads to a highly unstable training process, especially with the structured
 29 sparsity. For this reason, we impose limitations on the number of training iterations and the learning rate. Thus,
 30 we prioritize achieving reproducible and comparable results across all number formats over achieving full
 31 convergence for each specific configuration.

Table 4: Details of the sparse fine-tuning experiments

Model	Sparsity type	Batch size	Weight decay	Optimizer	FT num. iterations	Learning rate
OPT-125M	50%	8	-	Adam	1776	$1e^{-4}$
	2:4	8	-	Adam	1776	$1e^{-4}$
OPT-6.7B	50%	4	-	Adam	1000	$5e^{-4}$
	2:4	4	-	Adam	1500	$5e^{-4}$
LLaMA-2-7B	50%	2	$1e^{-3}$	AdamW	150	$2e^{-4}$
	2:4	2	$1e^{-3}$	AdamW	60	$5e^{-5}$
LLaMA-3-8B	50%	2	$1e^{-3}$	AdamW	200	$2e^{-5}$
	2:4	1	$1e^{-3}$	AdamW	300	$2e^{-5}$
ViT-B/16	50%	32	$1e^{-3}$	Adam	30000	$5e^{-5}$
	2:4	32	$1e^{-3}$	Adam	30000	$5e^{-5}$

32 OPT-125M and OPT-6.7B models are fine-tuned with block sizes of 512 and 1024 respectively, while LLaMa
 33 models utilize a block size of 2048. All configurations employ a linear learning rate schedule without a warm-up.

34 C Compute resources and runtime

35 We conduct our experiments on four NVIDIA A100 GPUs with 80GB memory, and for small models, we use
 36 four NVIDIA V100 GPUs with 32GB memory. The hyperparameters used in our experiments, including the
 37 number of fine-tuning epochs, are given in Appendix B. In summary, the estimated runtime for each fine-tuning
 38 experiments on these hardware platforms are as follows: (a) 20 minutes for OPT-125M, (b) 5-6 hours for
 39 OPT-6.7B, (c) 2-3 hours for LLaMA-2-7B and LLaMA-3-8B, and (d) 40 hours for ViT-B/16.

40 D Fine-tuning strategies

41 Magnitude-based sparsity applied in one-shot causes a significant perplexity degradation and thus needs an
 42 additional fine-tuning to recover the perplexity. In combination with quantization, several fine-tuning strategies
 43 are possible:

- 44 1. Sparse fine-tuning of FP32 model followed by the post-training quantization, sparsity masks are
 45 applied to the FP32 weight tensors
- 46 2. Fine-tuning in sparsified and quantized manner, where we sparsify and then quantize tensors at each
 47 iteration
- 48 3. Sparse fine-tuning of FP32 model followed by the post-training quantization, sparsity masks are
 49 applied to the quantized weight tensors
- 50 4. Fine-tuning in quantized and sparsified manner, where we quantize and then sparsify tensors at each
 51 iteration

52 The former two strategies correspond to the S→Q order of transformations, while the latter two correspond to
 53 the Q→S order. We conduct ablation experiments for the OPT-125M to compare these fine-tuning strategies.

The results are presented in the Table 5. According to our results, post-training quantization outperforms

Table 5: Validation perplexities of OPT-125M on WikiText2, produced by different fine-tuning strategies. The best results for each configuration are highlighted in bold.

Sparsity type	Number format	Order	Quantization during fine-tuning	PPL
50%	HBFP8	S→Q	×	30.46
			✓	33.51
		Q→S	×	39.04
			✓	37.48
50%	HBFP6	S→Q	×	32.51
			✓	36.20
		Q→S	×	41.97
			✓	40.86

54
55 sparse-and-quantized fine-tuning in S→Q order. In contrast, fine-tuning in quantized and sparsified manner
56 recovers perplexity better than post-training quantization in the reverse order.

57 E Post-training one-shot sparsity methods

58 Other sparsity schemes, such as Wanda and SparseGPT, have a different pruning policy, which uses activations
59 to assess the significance of the weights and prunes only the least significant ones. The pruning metrics in Wanda
60 and SparseGPT are

$$S_{ij} = |\mathbf{W}_{ij}| \cdot \|\mathbf{X}_j\|_2 \quad \text{and} \quad S_{ij} = \|\mathbf{W}\|^2 / \text{diag}((\mathbf{X}^T \mathbf{X} + \lambda \mathbf{I})^{-1})_{ij} \quad (27)$$

61 respectively. If quantization is applied before sparsity, the input values will change, which might also change the
62 set of the nullified weights. However, the significance of those weights will not change considerably. Therefore,
63 the correction vector $\tilde{\varepsilon}_c$ consists of the least significant weights, which are multiplied by the elements of $q(\mathbf{x})$
64 with the lowest values due to the chosen pruning metrics. As a result, the magnitude of ε_t and the effect of
65 changing the order of the operations is much lower for those sparsity schemes than for the magnitude-based
66 sparsity.

Table 6: OPT-125M and LLaMA-2-7B perplexities on WikiText2 for the combination of various number formats and sparsity schemes with both orders of operations.

Sparsity type	Sparsity method	Order	OPT-125M						LLaMA-2-7B					
			FP32	INT8	MXFP8	MXFP6	HBFP8	HBFP6	FP32	INT8	MXFP8	MXFP6	HBFP8	HBFP6
0%	-	-	27.65	28.06	28.45	28.01	27.81	29.91	5.12	5.15	5.17	5.16	5.12	5.24
50%	Magnitude	S→Q	29.94	30.22	31.13	31.20	30.46	32.51	6.31	6.94	6.40	6.38	6.32	6.51
		Q→S	-	34.71	36.39	35.60	37.48	40.86	-	8.13	8.47	9.32	9.86	10.20
	Wanda	S→Q	38.97	39.29	39.72	40.02	39.21	42.33	6.46	6.47	6.53	6.53	6.48	6.73
		Q→S	-	40.01	40.58	40.43	40.52	42.57	-	6.46	6.55	6.52	6.48	6.79
SparseGPT	S→Q	33.24	33.22	35.27	34.22	33.41	35.86	6.51	6.51	6.58	6.58	6.52	6.77	
	Q→S	-	33.54	35.32	34.29	33.64	36.80	-	6.53	6.60	6.58	6.55	6.93	
2:4	Magnitude	S→Q	31.89	32.76	33.99	33.41	32.25	34.58	9.30	9.37	9.35	9.32	9.39	10.68
		Q→S	-	45.06	44.16	42.25	46.57	55.64	-	14.65	14.35	14.50	14.98	18.64
	Wanda	S→Q	79.91	79.81	85.25	84.10	80.62	90.66	11.36	11.37	11.15	11.35	11.45	12.74
		Q→S	-	80.28	86.69	84.38	80.69	91.04	-	11.28	11.24	11.46	11.36	13.61
SparseGPT	S→Q	45.14	45.34	48.44	46.49	45.52	50.74	10.22	10.21	10.15	10.26	10.26	10.86	
	Q→S	-	44.96	48.67	46.50	45.82	57.39	-	10.21	10.24	10.26	10.21	11.16	

67 We further explore the effectiveness of post-training one-shot sparsity methods, specifically SparseGPT and
68 Wanda, which utilize a selection criterion based on the product of the magnitudes of weights and activations. We
69 report our results in Table 6 We observe that magnitude-based sparsity continues to achieve better perplexities
70 due to fine-tuning. However, because of their selection criterion, SparseGPT and Wanda are not affected by
71 the order of the operations. Even when quantization alters the relative magnitudes within a weight tensor, the
72 corresponding activations can compensate by preserving the original ranking of importance when multiplied
73 together. Consequently, the difference in perplexities between S→Q and Q→S for these methods is minimal,
74 and in few instances, Q→S yields better perplexities.

75 F Orthogonality bound for ViT

76 Table 7 shows the results of cross-entropy loss across various combinations of sparsity and quantization schemes
77 for ViT-B/16 performing the image classification task on ImageNet-1k. First, we note that the calculated

78 orthogonality bound serves as a correct lower bound for most configurations, supporting our theoretical analysis.
 79 Second, ViT-B/16 is significantly more robust to the combination of quantization and sparsity schemes compared
 80 to the other LLMs studied in this paper. When used with moderate sparsity levels (50% and 2:4) and 8-bit/6-bit
 81 number formats, the actual cross-entropy loss is close to the calculated orthogonality bound, showing the
 82 robustness of ViT-B/16. Only at higher compression rates achieved by using 75% or 1:4 sparsity and 4-bit
 83 number formats such as HBFP4, do we see the impact of the quantization and sparsity errors affecting the final
 cross-entropy loss, making it significantly higher than the calculated orthogonality bound.

Table 7: Comparison of evaluation cross-entropy loss with estimated orthogonality bounds

Sparsity type	Number format	ViT-B/16			
		Metric		Orthogonality Bound	
		Accuracy	CE Loss	Accuracy	CE Loss
0%	FP32	81.70%	0.703	-	-
	INT8	81.64%	0.706	-	-
	MXFP8	81.12%	0.722	-	-
	MXFP6	81.26%	0.715	-	-
	HBFP8	81.67%	0.704	-	-
	HBFP6	81.35%	0.718	-	-
	HBFP4	72.73%	1.094	-	-
50%	FP32	81.04%	0.723	-	-
	INT8	81.03%	0.728	80.98%	0.725
	MXFP8	80.50%	0.745	80.46%	0.742
	MXFP6	80.80%	0.734	80.60%	0.735
	HBFP8	81.00%	0.724	81.01%	0.723
	HBFP6	80.64%	0.736	80.69%	0.737
	HBFP4	73.38%	1.058	72.07%	1.113
2:4	FP32	80.06%	0.759	-	-
	INT8	79.95%	0.762	80.00%	0.761
	MXFP8	79.48%	0.781	79.48%	0.777
	MXFP6	79.73%	0.770	79.62%	0.771
	HBFP8	80.06%	0.760	80.03%	0.759
	HBFP6	79.69%	0.774	79.71%	0.773
	HBFP4	71.06%	1.163	71.09%	1.149
75%	FP32	77.26%	0.881	-	-
	INT8	77.03%	0.897	77.20%	0.884
	MXFP8	76.57%	0.913	76.68%	0.900
	MXFP6	76.99%	0.895	76.82%	0.894
	HBFP8	77.14%	0.882	77.23%	0.882
	HBFP6	76.89%	0.899	76.91%	0.896
	HBFP4	66.84%	1.365	68.29%	1.272
1:4	FP32	73.24%	1.055	-	-
	INT8	72.90%	1.070	73.18%	1.058
	MXFP8	72.36%	1.095	72.66%	1.074
	MXFP6	72.92%	1.070	72.80%	1.068
	HBFP8	73.16%	1.057	73.21%	1.056
	HBFP6	72.77%	1.078	72.89%	1.070
	HBFP4	59.58%	1.725	64.27%	1.446

84

85 G Layer-wise error analysis

86 Our mathematical study focuses on the per-layer error caused by the combination of quantization and sparsity. To
 87 demonstrate that this error is additive and increases with the layer index, we inspect the outputs of intermediate
 88 layers. In our experiment, we apply quantization and magnitude-based sparsity to all linear layers of the
 89 pre-trained OPT-125M model in a zero-shot manner. We feed a sample from a test subset to the compressed
 90 model and the corresponding full precision dense model and measure the difference between Feed-Forward
 91 outputs for each Transformer block. We repeat this experiment for S→Q and Q→S orders of transformations
 92 and show comparison results in Figure 1.

93 We observe that the per-layer error increases monotonically with layer index, regardless of the order of transfor-
 94 mations, and reaches its maximum value after the final layer. This error directly affects the output of the model
 95 and results in the metric degradation, which we have detected in the previous experiments 3.1, 3.2.

96 Layer-wise analysis also supports our theoretical findings that the optimal order of transformations is sparsity
 97 followed by quantization. The S→Q order of transformations consistently yields lower errors in the intermediate
 98 layer outputs compared to the reverse order. We observe an exponential increase in error with the Q→S order of
 99 transformations for the final layers, resulting in an error almost four times larger than with the optimal order.

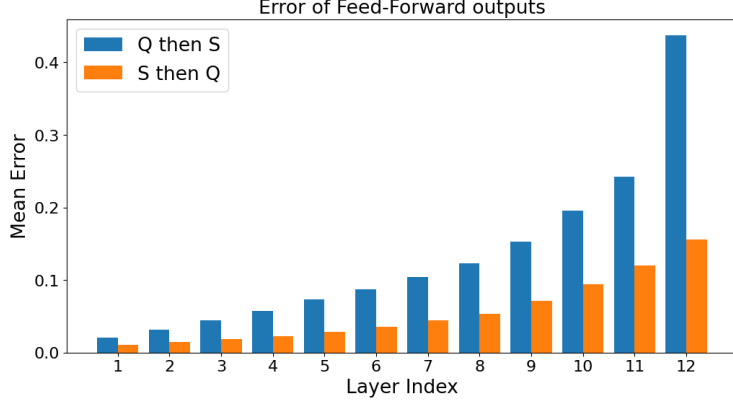


Figure 1: Per layer error of the combination of HBFP8 quantization and 2:4 structured sparsity

100 H Robustness analysis

101 To substantiate our conclusions on the optimal compression operation order, we conduct limited experiments
 102 across three distinct random seeds. We report the mean perplexities and error bars in the Table 8. Given the
 103 computational cost of fine-tuning, we limit the robustness analysis to the OPT-125M model and HBFP8/6
 104 number format. For both sparsity types we observe stable results, consistently affirming the higher efficacy of the
 S→Q order. Note that deviations caused by different seeds do *not* compromise the integrity of our conclusions.

Table 8: Validation perplexities of OPT-125M on WikiText2 for S→Q and Q→S. We report mean and standard deviation over three random seeds.

Sparsity Type	Number Format	Order	PPL
50%	HBFP8	S→Q	30.5 (± 0.2)
		Q→S	37.4 (± 0.3)
	HBFP6	S→Q	32.5 (± 0.2)
		Q→S	40.8 (± 0.3)
2:4	HBFP8	S→Q	32.2 (± 0.1)
		Q→S	46.5 (± 0.4)
	HBFP6	S→Q	34.6 (± 0.2)
		Q→S	55.5 (± 0.8)

105

106 I Proofs for the mathematical analysis

107 *Proof of Theorem 3.7.* Without loss of generality for simplicity we assume that the sparsity operation nullifies
 108 the last elements within the vector.

$$\|\varepsilon_{s \circ q}(\mathbf{x})\| = \left\| \begin{pmatrix} x_1 \\ \vdots \\ x_{n-n_s} \\ x_{n-n_s+1} \\ \vdots \\ x_n \end{pmatrix} - s \begin{pmatrix} x_1 - \varepsilon_q(\mathbf{x})_1 \\ \vdots \\ x_{n-n_s} - \varepsilon_q(\mathbf{x})_{n-n_s} \\ x_{n-n_s+1} - \varepsilon_q(\mathbf{x})_{n-n_s+1} \\ \vdots \\ x_n - \varepsilon_q(\mathbf{x})_n \end{pmatrix} \right\| = \left\| \begin{pmatrix} \varepsilon_q(\mathbf{x})_1 \\ \vdots \\ \varepsilon_q(\mathbf{x})_{n-n_s} \\ x_{n-n_s+1} \\ \vdots \\ x_n \end{pmatrix} \right\| \leq \quad (28)$$

$$\leq \left\| \begin{pmatrix} \varepsilon_q(\mathbf{x})_1 \\ \vdots \\ \varepsilon_q(\mathbf{x})_{n-n_s} \\ 0 \\ \vdots \\ 0 \end{pmatrix} \right\| + \left\| \begin{pmatrix} 0 \\ \vdots \\ 0 \\ x_{n-n_s+1} \\ \vdots \\ x_n \end{pmatrix} \right\| \leq \left\| \begin{pmatrix} \varepsilon_q^1 \\ \vdots \\ \varepsilon_q^{n-n_s} \\ \varepsilon_q^{n-n_s+1} \\ \vdots \\ \varepsilon_q^n \end{pmatrix} \right\| + \left\| \begin{pmatrix} 0 \\ \vdots \\ 0 \\ x_{n-n_s+1} \\ \vdots \\ x_n \end{pmatrix} \right\| = \quad (29)$$

$$= \|\varepsilon_q(\mathbf{x})\| + \left\| \begin{pmatrix} 0 \\ \vdots \\ 0 \\ x_{n-n_s+1} \\ \vdots \\ x_n \end{pmatrix} \right\| := \|\varepsilon_q(\mathbf{x})\| + \|\tilde{\varepsilon}_s(\mathbf{x})\| \quad (30)$$

109 When quantization is applied first, two distinct numbers can become the same: $x_i < x_j \rightarrow q(\mathbf{x})_i = q(\mathbf{x})_j$.
 110 When we sparsify the quantized numbers, the number that was smaller might get nullified, as depicted in Figure
 111 2. Therefore, the last component $\tilde{\varepsilon}_s$ of the upper bound does not equal ε_s .

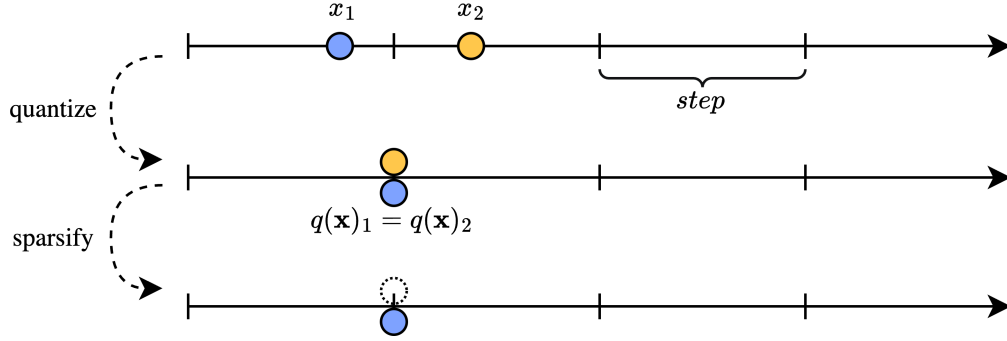


Figure 2: A visual representation of applying quantization first and then sparsification. After quantization two distinct elements become equal. Then, when sparsification is applied, the element that was originally bigger gets nullified as the sparsification operation cannot differentiate them by their magnitude.

112 However, in this case we can get an upper bound for the distance between them:

$$\begin{cases} x_i < x_j \\ q(\mathbf{x})_i \geq q(\mathbf{x})_j \end{cases} \Leftrightarrow \begin{cases} x_i < x_j \\ x_i - \varepsilon_q(\mathbf{x})_i \geq x_j - \varepsilon_q(\mathbf{x})_j \end{cases} \Leftrightarrow \begin{cases} x_j - x_i > 0 \\ x_j - x_i \leq \varepsilon_q(\mathbf{x})_j - \varepsilon_q(\mathbf{x})_i \end{cases} \Rightarrow \quad (31)$$

$$\Rightarrow |x_j - x_i| \leq |\varepsilon_q(\mathbf{x})_j - \varepsilon_q(\mathbf{x})_i| \leq |\varepsilon_q(\mathbf{x})_j| + |\varepsilon_q(\mathbf{x})_i| \leq 2 \cdot \text{step} \quad (32)$$

113 For each x_i that was nullified after quantization followed by sparsification we define x_i^t to be an element that
 114 would be nullified, if quantization was not applied. Then the vector $\varepsilon_s(\mathbf{x})$ consists of all and only such elements
 115 x_i^t .

116 There exists a permutation W of the vector $\varepsilon_s(\mathbf{x})$ such that maps the element x_i in $\tilde{\varepsilon}_s(\mathbf{x})$ to the element x_i^t in
 117 $\varepsilon_s(\mathbf{x})$. This helps us to get an optimal upper bound for the additional error:

$$\|\tilde{\varepsilon}_s(\mathbf{x})\| = \|\tilde{\varepsilon}_s(\mathbf{x}) - W\varepsilon_s(\mathbf{x}) + W\varepsilon_s(\mathbf{x})\| \leq \|W\varepsilon_s(\mathbf{x})\| + \|\tilde{\varepsilon}_s(\mathbf{x}) - W\varepsilon_s(\mathbf{x})\| = \quad (33)$$

118

$$= \|\varepsilon_s(\mathbf{x})\| + \left\| \begin{pmatrix} 0 - 0 \\ \vdots \\ 0 - 0 \\ x_{n-n_s+1} - x_{n-n_s+1}^t \\ \vdots \\ x_n - x_n^t \end{pmatrix} \right\| \leq \|\varepsilon_s(\mathbf{x})\| + \left\| \begin{pmatrix} 0 - 0 \\ \vdots \\ 0 - 0 \\ 2 \cdot \text{step} \\ \vdots \\ 2 \cdot \text{step} \end{pmatrix} \right\| \quad (34)$$

119 For the case of $N : M$ sparsity then number of nullified elements within the block equals $\frac{M-N}{M} \cdot n$. Therefore,
 120 with respect to L_1 norm, the last error term can be evaluated as follows:

$$\left\| \begin{pmatrix} 0 - 0 \\ \vdots \\ 0 - 0 \\ 2 \cdot \text{step} \\ \vdots \\ 2 \cdot \text{step} \end{pmatrix} \right\|_1 = 2 \cdot \text{step} \cdot \frac{M - N}{M} \cdot n \quad (35)$$

121

□

122 *Proof of Theorem 3.9.* To prove non-orthogonality, consider the blocks of floating-point numbers $x =$
 123 $(1.0, 1.0)^T$, $w = (0.6, 1.3)^T$, HBF4 quantization q and 1:2 sparsity s . We assume that q does not affect x :
 124 $q(x) = x$. On the other hand, the block w is transformed in the following way:

$$s(\mathbf{w}) = \begin{pmatrix} 0 \\ 1.3 \end{pmatrix} \quad q(\mathbf{w}) = \begin{pmatrix} 0.625 \\ 1.25 \end{pmatrix} \quad s(q(\mathbf{w})) = s(q(\mathbf{w})) = c(\mathbf{w}) = \begin{pmatrix} 0 \\ 1.25 \end{pmatrix} \quad (36)$$

125 The dot product error of the composition equals:

$$\varepsilon_{q,c}^D(\mathbf{x}, \mathbf{w}) = \langle \mathbf{x}, \mathbf{w} \rangle - \langle q(\mathbf{x}), c(\mathbf{w}) \rangle = \left\langle \begin{pmatrix} 1.0 \\ 1.0 \end{pmatrix}, \begin{pmatrix} 0.6 \\ 1.3 \end{pmatrix} \right\rangle - \left\langle \begin{pmatrix} 1.0 \\ 1.0 \end{pmatrix}, \begin{pmatrix} 0 \\ 1.25 \end{pmatrix} \right\rangle = 0.65 \quad (37)$$

126 The dot product error of quantization equals:

$$\varepsilon_q^D(\mathbf{x}, \mathbf{w}) = \langle \mathbf{x}, \mathbf{w} \rangle - \langle q(\mathbf{x}), q(\mathbf{w}) \rangle = \left\langle \begin{pmatrix} 1.0 \\ 1.0 \end{pmatrix}, \begin{pmatrix} 0.6 \\ 1.3 \end{pmatrix} \right\rangle - \left\langle \begin{pmatrix} 1.0 \\ 1.0 \end{pmatrix}, \begin{pmatrix} 0.625 \\ 1.250 \end{pmatrix} \right\rangle = 0.025 \quad (38)$$

127 The dot product error of sparsity equals:

$$\varepsilon_{I,s}^D(\mathbf{x}, \mathbf{w}) = \langle \mathbf{x}, \mathbf{w} \rangle - \langle \mathbf{x}, s(\mathbf{w}) \rangle = \left\langle \begin{pmatrix} 1.0 \\ 1.0 \end{pmatrix}, \begin{pmatrix} 0.6 \\ 1.3 \end{pmatrix} \right\rangle - \left\langle \begin{pmatrix} 1.0 \\ 1.0 \end{pmatrix}, \begin{pmatrix} 0 \\ 1.3 \end{pmatrix} \right\rangle = 0.6 \quad (39)$$

128 Therefore, for these particular values of \mathbf{x} and \mathbf{w} , the inequality: $|\varepsilon_{q,c}^D(\mathbf{x}, \mathbf{w})| > |\varepsilon_q^D(\mathbf{x}, \mathbf{w})| + |\varepsilon_{I,s}^D(\mathbf{x}, \mathbf{w})|$
 129 holds true.

130

□

131 J Definitions of Q for numerical formats

132 1. INT m (Symmetric version) [8]

$$Q_m(x_i, \text{scale}) = s \cdot \left\lfloor \frac{x_i}{s} \right\rfloor, \text{ where } s = \frac{\text{scale}}{2^{m-1} - 1}, \quad (40)$$

133 2. HBF4 m [11]

$$Q_m(x_i, \text{scale}) = s \cdot \left\lfloor \frac{x_i}{s} \right\rfloor, \text{ where } s = 2^{\lceil \log_2(\text{scale}) \rceil - (m-1)} \quad (41)$$

134 3. MXFP m [5] [41]

$$135 \quad Q_m(x_i, \text{scale}) = \text{scale} \cdot (-1)^S \cdot 2^E \cdot (1 + 2^{-m} \cdot M) \quad (42)$$

$$\text{where } S = \text{sign}(x_s) \quad (43)$$

$$E = \lceil \log_2(|x_s|) \rceil - \text{bias} \quad (44)$$

$$M = \left\lfloor \left(\frac{|x_s|}{2^E} - 1 \right) \cdot 2^m \right\rfloor \quad (45)$$

$$x_s = \frac{x}{2^{\lceil \log_2(\text{scale}) \rceil}} \quad (46)$$

$$(47)$$

136 Value of *bias* depends on the chosen configuration [39].

137 4. MXINT m [5] [41]

$$Q_m(x_i, \text{scale}) = s \cdot \left\lfloor \frac{x_i}{s} \right\rfloor, \text{ where } s = 2^{\lceil \log_2(\text{scale}) \rceil - (m-1)} \quad (48)$$

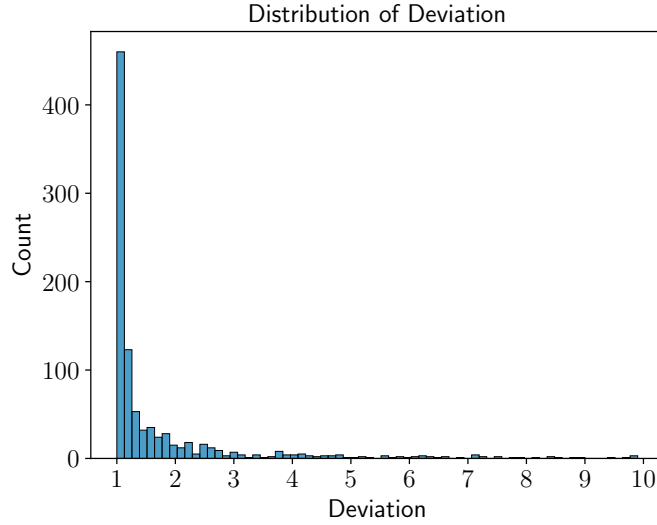


Figure 3: Distribution of the deviation values for several random blocks.

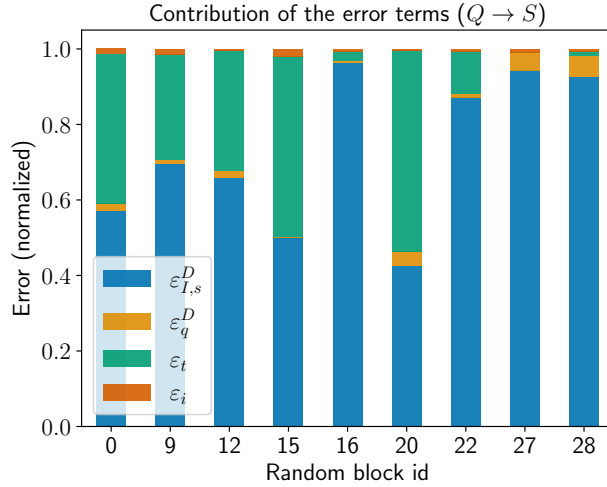


Figure 4: Normalized values of each error term of the upper bound for the case of applying quantization before sparsity.

138 **K Analysis of the upper bound of the dot product error**

139 **K.1 Upper bound is reachable**

140 To test if the upper bound derived in Theorem 3.9 is reachable in practice, we randomly sampled 1000 blocks of
 141 size 64 from a standard normal distribution $\mathcal{N}(0, 1)$, and applied 2:4 sparsity and HBFP6 quantization. We then
 142 compute the aggregate error of the composition and individual error term of the upper bound. Subsequently, we
 143 quantified how much the upper bound deviates from the actual composition error using the following formula:

$$\text{Deviation} = \frac{|\varepsilon_{I,s}^D(\mathbf{x}, \mathbf{w})| + |\varepsilon_q^D(\mathbf{x}, \mathbf{w})| + |\varepsilon_t| + |\varepsilon_i|}{|\varepsilon_{q,c}^D(\mathbf{x}, \mathbf{w})|} \quad (49)$$

144 As a corollary of Theorem 3.9, the minimal value of deviation is 1.

145 Figure 3 shows the deviation distribution of samples. Most values fall into the first bin, suggesting the upper
 146 bound is frequently reached. It can also be seen that the deviation values can be large, almost reaching the value
 147 of 10, which indicates that the upper bound can be pessimistic in some cases too. Theorem 3.9 does not rule out

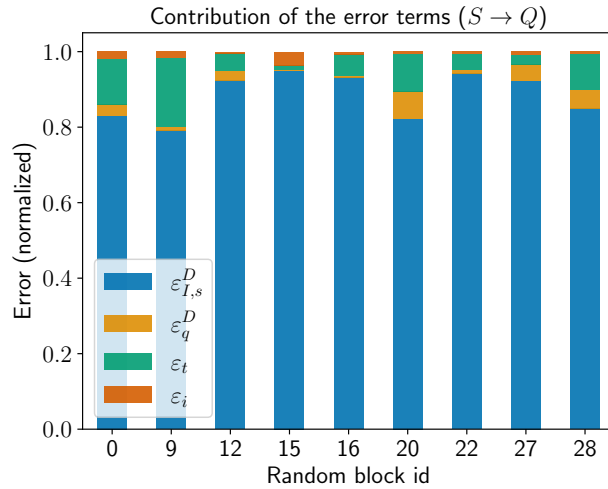


Figure 5: Normalized values of each error term of the upper bound for the case of applying sparsity before quantization. We fix the seed and consider the same random blocks as for the order $Q \rightarrow S$.

148 large values of deviation, as it applies the triangle inequality to obtain the upper bound, which leads to dropping
 149 the sign of each error term. If the values of the error terms are negative, they can make the overall error of the
 150 composition lower than the upper bound, which leads to the deviation values larger than one.

151 K.2 Contribution of additional error terms

152 Section 3.2 describes how each additional error term can contribute to the overall error of the composition. We
 153 hypothesize that the error term ϵ_t contributes less in case of applying sparsity followed by quantization than in
 154 case of applying quantization first. We also hypothesize that the magnitude of the error term ϵ_i is much lower
 155 than the magnitude of ϵ_t . To test our hypotheses, we normalized the values of each term of the upper bound to
 156 compare their contribution to the error. We considered both orders of applying the transformations. We also
 157 only looked at the samples with low deviation values (< 1.05) to increase the explainability power of the upper
 158 bound.

159 Figures 4 and 5 depict the results of the experiment. If we consider the order $Q \rightarrow S$ in Figure 4, we can see
 160 that the term ϵ_t advocates for almost half of the error of the composition. However, in the order $S \rightarrow Q$ the
 161 term ϵ_t has a much lower impact, which proves our first hypothesis.

162 We can also see that the values of ϵ_i are much lower than the values of ϵ_t in most of the cases in both orders.
 163 This proves our second hypothesis.